REVIEW PAPER

Electric Field Control of Fe Nano Magnets: Towards Metallic Nonvolatile Data Storage Devices

Toyo Kazu Yamada[1,2]*, Lukas Gerhard[1], Timofey Balashov[1], Albert F. Takács[1,3],
Rien J. H. Wesselink[1], and Wulf Wulfhekel[1]

[1]*Physikalisches Institut, Karlsruhe Institute of Technology (KIT), 76131 Karlsruhe, Germany*
[2]*Graduate School of Advanced Integration Science, Chiba University, Chiba 263-8522, Japan*
[3]*Faculty of Physics, Babes-Bolyai University, 400084 Cluj-Napoca, Romania*

Magnetoelectric coupling at metal surfaces opens up a new possibility for metallic nonvolatile magnetic data-storage devices, in which the magnetic bits are controlled by an electric field. We studied the atomic and magnetic order in bilayer Fe nano-islands grown on a Cu(111) substrate with a scanning tunneling microscopy setup in ultra high vacuum at 4.5 K. Electric field pulses (10^8–10^9 V/m) were found to be able to cause a displacement of the Fe atoms, switching simultaneously the crystalline and the magnetic order, which is the prove of magnetoelectric coupling at the metallic Fe surface. We also succeeded in controlling the direction of the switching by the polarity of the electric field.
© 2011 The Japan Society of Applied Physics

1. Introduction

The construction of a ubiquitous network society relies on the drastic development of data-storage devices with low power consumption, increasing speed and bit density. The realization of such near-future devices will be possible if reading, writing, and storing information processes, such as in hard disks, are performed by electric fields. Currently magnetic fields used to controlling each nano-magnet inside data-storage devices are energy consumptive due to the current that is flowing through the coils. Furthermore, the magnetic stray field limits the size of the magnetic bits to be written and the magnetic anisotropy needed for small stable bits cannot be overcome by magnetic fields anymore. These limitations can be avoided when using magnetoelectric coupling in magnetic storage devices.

Materials in which magnetic order can be controlled by electric fields have been already studied for a long time, while they are usually insulators such as $TbMnO_3$,[1] $HoMnO_3$,[2] $BaTiO_3$,[3] $BiFeO_3$,[4] and have complicate structures, making it difficult to fabricate practical devices. If one finds such phenomena in simple metals, this will be a big step towards a realization of electrically controlled magnetic devices as metals have been widely used in recent magnetic data-storage devices.

The electric field can induce charges on the surface of metals, which may shift the atomic position. If this subtle displacement changes the magnetic order, the material displays a magnetoelectric coupling. In general, electric fields cannot penetrate bulk metals, because they are screened by the conduction electrons. However, the influence of an electric field becomes detectable if the thickness of the metal is reduced to the nanometer scale. Recently, controlling the magnetic anisotropy by the electric field was reported for the Fe/MgO junctions.[5]

A necessary condition to find magnetoelectric coupling in metals is that the metal possesses a close interaction between crystalline and magnetic structure. Iron is one of the metallic magnets in which the magnetic order is very sensitive to the crystalline structure. A subtle displacement of the inter-atomic distances causes a wide variety of spin configurations even in bulk.[6,7]

Iron in bulk is a typical bcc-metal at room temperature, but it takes the fcc γ-phase at 1185–1667 K and the bcc δ-phase at 1667–1811 K, indicating a small energy barrier between bcc and fcc phases.[8] Bcc Fe in bulk is ferromagnetic, but fcc Fe in bulk does not have a stable ferromagnetic phase.[6,7] The energy balance of the phases can be modified. Especially at surfaces, interfaces and nanometer scale regimes, the phase diagram of iron is drastically changed due to the break of symmetry, causing unique features. Recently, a surface reconstruction on the surface of a bcc-Fe(110) whisker single crystal was found,[9] where the top atomic layer has a fcc(111)-like quasi-hexagonal symmetry and interacts with the sub-surface bcc(110) symmetry, causing a Moiré-like pattern. In Fe nano-islands grown on a Cu(111) substrate, the coexistence of bcc(110) and fcc(111) phases was found.[10] This indicates that the barrier between the phases becomes smaller at the surface or in nanometer scale regimes, especially along the bcc ⟨110⟩ orientation which is the most dense-packed in bcc.

In this study, we applied electric field to the nanometer-scale bilayer Fe islands grown on a Cu(111) single crystal with a scanning tunneling microscopy (STM) setup in ultra-high vacuum at 4.5 K. We studied the crystalline and magnetic structure of the two phases in the Fe nano-islands and succeeded to characterize them: (1) The bcc structure is ferromagnetic and (2) the fcc structure is layer-wise antiferromagnetic. Applying a high electric field to the Fe nano-islands induces subtle displacements of the atomic positions, changing the crystalline and the magnetic order simultaneously.[11,12] Statistical experiments showed that the polarity of the electric field allows selective switching from one phase to the other and *vice versa*. This new finding of a magnetoelectric coupling at the metallic Fe surface will rise new hope towards an electric field controlled magnetic data-storage device.[13]

2. Experimental Methods

Fe nano-islands were grown in a ultrahigh vacuum (UHV) preparation chamber. Its base pressure is below 5×10^{-8} Pa. The Cu(111) single crystal was sputtered by Ar ions at 300 K and subsequently annealed up to 450 K. Repetitions of the sputtering and annealing cycles result in a clean and atomically flat Cu surface. Afterwards 0.2 monolayers of Fe, purity 99.995%, were deposited from an electron-bombardment type evaporator onto the Cu(111) substrate at 300 K.

*E-mail address: toyoyamada@faculty.chiba-u.jp

The fabricated samples were studied in our scanning tunneling microscope at 4.5 K in UHV. Topographic images and atomically resolved STM images were obtained using non-magnetic tungsten tips. Local density of states (LDOS) and magnetic information at each position were obtained by scanning tunneling spectroscopy (STS) as well as spin-polarized STM/STS techniques with W tips and spin-polarized Fe/W tips.[14–17] Experimentally obtained differential tunneling conductivity (dI/dV) curves were normalized by its fitted tunneling probability functions (T) to recover the LDOS.[11,18–20]

3. Results and Discussion

3.1 Atomic and spin configurations in the Fe nano islands

Figure 1 shows a topographic STM image ($80 \times 50\,\text{nm}^2$) obtained on the surface of 0.2 MLs of Fe deposited on the clean Cu(111) single crystal substrate. Fe forms bilayer islands with sizes of 5–20 nm. Due to the symmetry of the fcc substrate, the islands preferentially grow in a triangular-like shape.[21] These nano-islands do not consist of a single phase, but exhibit a coexistence of bcc and fcc structures.[10] The bcc area appears brighter (black circle in Fig. 1) and the fcc area appears darker (white circle in Fig. 1). The height difference is about 30 pm.

Figure 2 shows an atomically resolved STM image (4×4 nm^2) at the boundary between bcc and fcc areas. The white line indicates the boundary. The red lattice indicates the hexagonal symmetry of the fcc(111) substrate, which fits well the atomic positions at the fcc area, but not at the bcc area. Sphere models at the bcc and the fcc areas, depicted in Fig. 2, show that the top-layer atoms of a fcc(111) surface area sit on the three-fold hollow sites of the sub-surface Fe layer, while the atoms of a bcc(110) surface sit on the bridge sites. This is why there is not only an in-plain atomic displacement but also an out-of-plain displacement necessary to complete the transition from fcc to bcc. The in-plain displacement can be observed as a 5.3° tilt of the atomic lattice directions while the out-of-plain displacement results in the height difference of the two phase of about 30 pm. Hence our STM images directly give the information about a possible phase transition that might be induced by an electric field.

To identify the magnetic order of the two phases, however, need a more sophisticated approach. As we will
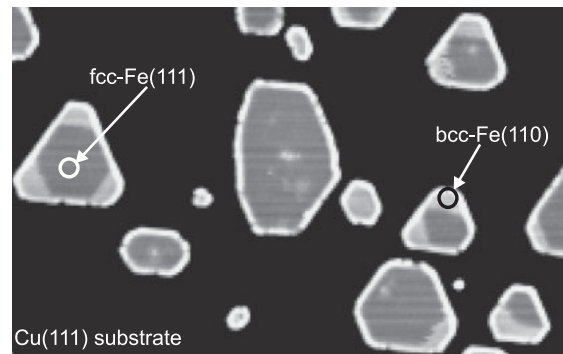

Fig. 1. An STM topographic image ($80 \times 50\,\text{nm}^2$) obtained on the surface of 0.2 MLs of Fe on a clean Cu(111) single crystal substrate. Brightness denotes height. The white and black circles indicate areas with the fcc(111) and the bcc(110)-like structure, respectively. The height difference between the areas is about 30 pm.

see, the magnetic order does not remain the same as in the bulk ground state, i.e., ferromagnetic, but is different for the two phases. In order to investigate the spin configuration of the bcc and fcc phase in the bilayer Fe nano-islands a combination of experimental STS, spin-polarized STM measurements and theoretical *ab-initio* calculations[11] was performed.

Our spin-polarized STM measurements confirmed that there is no spin variation in the top layer, i.e., we have to focus on possible magnetic structures in which the spins of the top layer point the same direction.

Normalized differential tunneling conductivity [(dI/dV)/T] curves, which correspond to the LDOS, obtained on the bcc and the fcc area are shown in Fig. 3. These show that the LDOS near the Fermi energy is quite sensitive to the crystalline structure. The bcc(110)-like area has a sharp LDOS peak around -0.2 V, but the fcc(111)-like area has three peaks at -0.4 V, near the Fermi energy, and at $+0.3$ V. Our theoretical calculations revealed that the LDOS peaks strongly depend on the spin configuration between the top and sub-surface layers.[11] For example, the layer-wise ferromagnetic coupling in the fcc scheme produces a strong LDOS peak at $+0.2$ V, which does not fit our experimentally obtained LDOS at the fcc area, i.e., the spins in the fcc area don't couple ferromagnetically between layers. A compar-
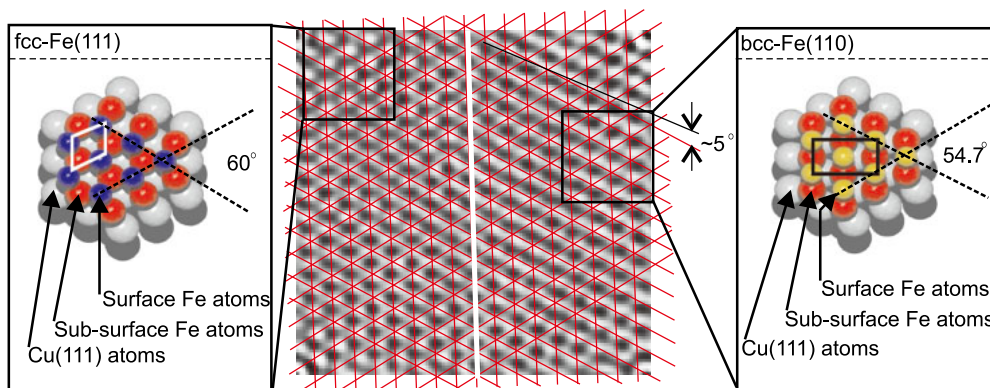

Fig. 2. (Color online) An atomically resolved STM image ($4 \times 4\,\text{nm}^2$) obtained at the boundary between the fcc and the bcc areas. The red lattice is a guides to the eyes, showing the hexagonal symmetry of the fcc(111) Cu surface. The white line indicates the boundary, where the atomic lattices tile about 5 degrees. Sphere models show a top view of the atomic positions at each area.
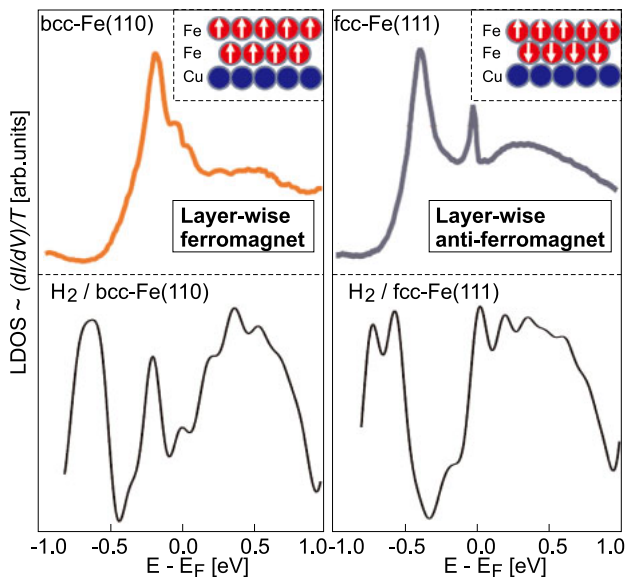
Fig. 3. (Color online) Upper panels show differential tunneling conductivity (dI/dV) curves normalized by its fitted tunneling probability (T) curves, corresponding to the local density of states (LDOS), obtained at bcc(110)- and fcc(111)-like areas on the Fe nano-islands. Insets indicate the cross section views of sphere models.[11] Arrows indicate magnetic moments of each Fe atom. Lower panels show LDOS obtained on the same area after introducing a does of 2 L of hydrogen gas (see Supplementary Information in ref. 11).

ison between the experimentally obtained LDOS and the calculated LDOS with various spin configurations allows us to recover the true spin configuration of the bcc and the fcc areas: The bcc area has a ferromagnetic state and the fcc area has a layer-wise antiferromagnetic state, i.e., the bcc and the fcc area of the Fe nano-islands have different spin configurations.

Before performing any experiments related to magneto-electric coupling, one has to rule out influence on the Fe surfaces by impurities since the 3d metal surfaces are relatively active compared to the noble metals, binding easily with impurities such as oxygen[22] or hydrogen[11] atoms. Oxygen atoms were usually observed as dark depressions (5–10 pm in depth) in the STM images due to the quench and slight shift of the 3d surface states.[22] In our STM experiments, we observed such dark depression rarely and estimated the concentration much lower than 0.1%. Concerning possible hydrogen impurities, our experimental data of hydrogen atoms on Pt(111) surface and the sticking coefficient difference between Fe and Pt[11] give us a concentration of hydrogen of less than 0.1%. We also checked the consequences of a deliberate hydrogen contamination of the iron surface by introducing a dose of 2 L (L = Torr·s) hydrogen into the UHV chamber. An STM image shows the resulting H-(2 × 2) superstructure on the surface and the drastic change of the experimental LDOS (Fig. 3[11]). With this, we are sure that the surface of the Fe nano-islands is clean in the sense, that we can perform reliable switching experiments without regarding a possible influence due to contaminations.

3.2 Electric field controlling the Fe nano magnets
Our theoretical calculations predict that a huge electric field of the order of 10^9 V/m is needed to trigger the crystal-

lographic and magnetic phase transition.[11,12] An STM setup can produce such large electric fields: Since the gap distance between the STM probe tip and the sample surface is smaller than 1 nm, a bias voltage of the order of 1 V generates an electric field of more than 10^9 V/m. In this study, we applied electric fields of 10^6–10^{10} V/m to the Fe nano-islands.

Figure 4 shows a Fe nano-island including ferromagnetic bcc and antiferromagnetic fcc areas. First, we obtained an STM image under a low electric field ($\sim10^7$ V/m) (left panel), where the center area of the island is in the ferromagnetic (FM) bcc state. Subsequently, the STM probe was moved to the center of the island (cross in the sketch) and a voltage pulse (10^9 V/m) within 50 ms was applied. Then again, a STM image was taken under a low electric field (right panel). Now the center area of the Fe nano-island is in the antiferromagnetic fcc state, i.e., we experimentally succeeded to switch the magnetic states of the metallic Fe nano-islands by an electric field from ferromagnetic bcc to antiferromagnetic fcc which is the first prove of magneto-electric coupling at metal surfaces. Depending on the size of electric field, we succeeded to switch a whole island or a very small area of about 1 nm^2 (see the demonstration in ref. 11). If each area of 1 nm^2 represents one bit of information, this will give us a data-storage device with an extremely high density of more than 10^{12} bits/inch^2. So far, we confirmed that the switching is possible with a pulse as short as 0.06 ms, which is the time resolution of our STM setup (see Supplementary Information in ref. 11). Much faster response time for the switching is expected, which is an exciting aspect in the view of future applications.

Using an STM setup, we must take into account the influence of the tunneling current. In Fig. 5, the experimentally obtained relation between critical voltages and tunneling current values, where the phase switching occurs, is plotted as black triangles (details of the measuring method are shown in ref. 12). We tried to fit this by equations for the critical voltage as a function of the tunneling current based on different possible models for the switching. This way we want to make sure whether the origin of the switching is the electric field or not. Five different possibilities for the switching mechanism are considered: (1) spin torque effect[23] or spin accumulation,[24] or electro-migration, (2) inelastic spin scattering,[25] (3) local heating, (4) mechanical interaction or chemical bonding with the tip, and finally (5) the electric field.[11,12]

(1) Spin torque, spin accumulation, and electro-migration are determined by the number of electrons, thus the switching occurs at a certain constant tunneling current ($I = I_c$, dashed line in Fig. 5). (2) Inelastic tunneling electrons could excite the spin state of the Fe nano-clusters at a particular bias voltage, which may change the spin order. Then the switching occurs at a constant bias voltage ($V = V_c$, red line in Fig. 5). (3) It could be that the switching relates to a thermal phase transition due to very local heating under the tip. In such case the switching occurs at a constant power ($P = P_c$, i.e., V is proportional to I^{-1}, green line in Fig. 5). (4) The mechanical or chemical interaction between the tip and the sample is due to the overlap of the wave functions that is proportional to the tip–sample distance (z). Since the tunneling current can be described as $I \propto$
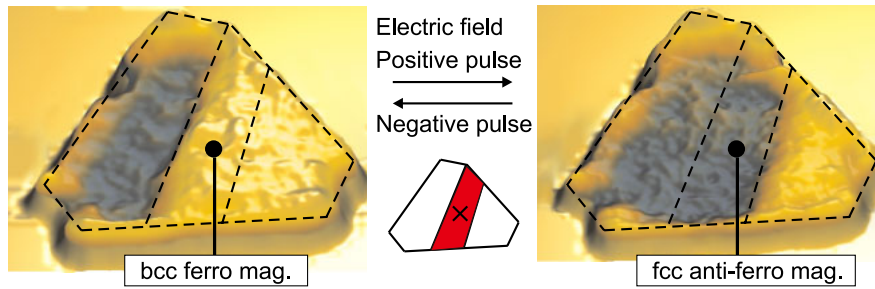
Fig. 4. (Color online) STM topographic images obtained on the same single Fe nano-island before and after the application of a electric field pulse. The field was applied at the center of the island (×). The area colored in red changes the phase, showing magnetoelectric coupling at the Fe surface.
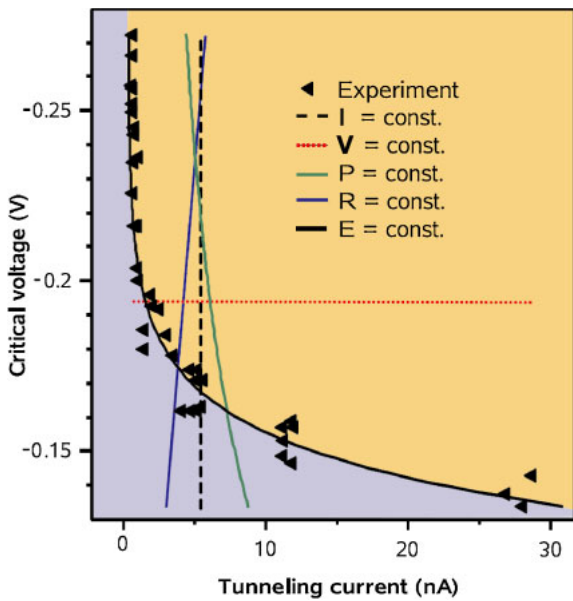

Fig. 5. (Color online) A systematic study to find the origin of the phase switching. Experimentally obtained critical tunneling current and bias voltages, where the phase switch occurs, are plotted as triangles. Four possible origins where the switching occurs at (1) constant tunneling current ($I = I_c$, dashed line), (2) constant bias voltage ($V = V_c$, red line), (3) constant power ($P = P_c$, green line), and (4) constant tip–sample distance or resistance ($R = R_c$, blue line) do not fit to the experimental data. Only, (5) the constant electric field model fits the experimental data well, proving that the origin of the switching is the electric field ($E = E_c$, black line).

$V \exp(-2\kappa z)$, where κ is the decay constant,[19] a constant distance corresponds to a constant resistance $R = V/I \propto \exp(2\kappa z) \propto R_c$ (blue line in Fig. 5). In summary, Fig. 5 clearly shows that these four possible origins: (1)–(4) do not fit to the experimentally obtained values (triangles), excluding these possibilities as the origin of the phase switching. (5) If the phase switching occurs at a constant electric field ($E = E_c$), the tunneling current formula $I \propto V \exp(-2\kappa z)$ can be described as $I \propto V \exp(-cV)$ with $E = E_c = V/z$, i.e., $V \propto z$ (c: coefficient). With this we succeeded to fit our experimental data well (black line in Fig. 5), proving the origin of the switching to be the electric field.

Quantitatively, the amplitude of the electric field causing the phase switching is able to get from the experimental data since the tunneling conductance, $I \propto V \exp(-2\kappa z)$, can be described as $I = G_0 V$ when the tip contacts to the Fe nano-islands ($z = 0$), where G_0 denotes the quantum conductance

of $2e^2/h = 1/(12.9 \, \text{k}\Omega)$. Thus the tunneling current can be described as $I = G_0 V \exp(-2\kappa z)$ at $z \neq 0$. Since experimentally we know the switching values of I and V, we can get z at each set of data. If we re-plot the data in the V–z plane,[11] its slope corresponds to the critical electric field. We got $E_c = (3\text{–}9) \times 10^8$ V/m.

For controlling the phase switching one to the other, the vector quantity of the electric field is one of the most important key issues. Depending on the polarity of the electric field, negative or positive charges are induced on the tip apex, which pull or push the Fe atomic nucleus and therefore determine whether the ferromagnetic bcc or the antiferromagnet fcc state is favoured. Theoretical calculations found that atomic and spin orders strongly depend on the polarity of the electric field.[11,12] The energetically most stable configuration was the antiferromagnetic fcc state for the positive electric field and the ferromagnetic bcc state for the negative electric field. This theoretical prediction can be confirmed experimentally by statistical switching experiments. We repeated very similar experiments as Fig. 4, so positive or negative electric field pulses were applied to the Fe nano-islands and checked whether the state changed after the pulse (64 times with positive field and 49 times with negative field).

The theoretical calculations[11,12] predict the energy landscape of the bilayer Fe nanoislands. Under a positive electric field, the fcc antiferromagnetic (AFM) state is energetically stable, so the barrier from this state to the bcc FM state is ~40 meV higher than that from the bcc FM to the fcc AFM state. We tried to switch the bcc FM area to the fcc AFM state 40 times and we succeeded to switch 38 times by applying positive electric field pulses, but only two out of 24 trials succeeded in the case of switching from the fcc AFM to the bcc FM state by a positive electric field (see upper panel in Fig. 6), which fits pretty well to the theory.[11,12] This also shows that the fcc AFM state is practically stable under the positive electric field. The same procedures were also performed for the case of a negative electric field (lower panel in Fig. 6). The calculated energy landscape showed that the energy barrier from the bcc FM to the fcc AFM state is more than 100 meV,[11,12] which was confirmed by our experiments, so under the negative field, we succeeded to switch from the fcc AFM to the bcc FM state 22 times out of 24 trials and never succeeded to switch from the bcc FM to the fcc AFM state (0 out of 25 trials), which indicates that experimentally the bcc FM state is stable under a negative electric field.
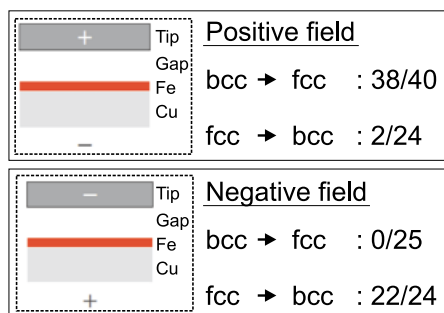
Fig. 6. (Color online) Statistical experiments proved that the fcc antiferromagnetic (AFM) and the bcc ferromagnetic (FM) state switch to the other state only under negative and positive electric fields, respectively. "38/40" indicates that the switching succeeded 38 times out of 40 trials. Insets show a sketch of the STM tunnel junction, where + and − denote the induced positive and negative charges.

These statistical experiments give us important information about how to control the switching of the magnetic states in the Fe nano-islands by the polarity of the electric field.

4. Conclusions

We studied bilayer Fe nano-islands (5–20 nm in size) grown on a Cu(111) single crystal by means of STM and spin-polarized STM/STS in UHV at 4.5 K. We experimentally confirmed that the magnetic state in the Fe nano-islands can be controlled by electric fields of 10^8–10^9 V/m, i.e., magnetoelectric coupling exists at the metal surface. A positive electric field favors the transition from the ferromagnetic bcc to the antiferromagnetic fcc state, and a negative electric field favors the transition from the antiferromagnetic fcc to the ferromagnetic bcc state. These new findings make it possible to read, write and store information in metallic magnets by an electric field. This is a breakthrough towards the realization of new classes of electric field controlled magnetic data-storage devices.

1) T. Kimura, T. Goto, H. Shintani, K. Ishizaka, T. Arima, and Y. Tokura: Nature **426** (2003) 55.
2) T. Lottermoser, T. Lonkai, U. Amann, D. Hohlwein, J. Ihringer, and M. Fiebig: Nature **430** (2004) 541.
3) H. Zheng, J. Wang, S. E. Lofland, Z. Ma, L. Mohaddes-Ardabili, T. Zhao, L. Salamanca-Riba, S. R. Shinde, S. B. Ogale, F. Bai, D. Viehland, Y. Jia, D. G. Schlom, M. Wuttig, A. Roytburd, and R. Ramesh: Science **303** (2004) 661.
4) F. Zavaliche, H. Zheng, L. Mohaddes-Ardabili, S. Y. Yang, Q. Zhan, P. Shafer, E. Reilly, R. Chopdekar, Y. Jia, P. Wright, D. G. Schlom, Y. Suzuki, and R. Ramesh: Nano Lett. **5** (2005) 1793.
5) T. Maruyama, Y. Shiota, T. Nozaki, K. Ohta, N. Toda, M. Mizuguchi, A. A. Tulapurkar, T. Shinjo, M. Shiraishi, S. Mizukami, Y. Ando, and Y. Suzuki: Nat. Nanotechnol. **4** (2009) 158.
6) G. L. Krasko and G. B. Olson: Phys. Rev. B **40** (1989) 11536.
7) V. L. Moruzzi, P. M. Marcus, K. Shwarz, and P. Mohn: Phys. Rev. B **34** (1986) 1784.
8) H. Hasegawa and D. G. Pettifor: Phys. Rev. Lett. **50** (1983) 130.
9) T. K. Yamada, H. Tamura, M. Shishido, T. Irisawa, and T. Mizoguchi: Surf. Sci. **603** (2009) 315.
10) A. Biedermann, W. Rupp, M. Schmid, and P. Varga: Phys. Rev. B **73** (2006) 165418.
11) L. Gerhard, T. K. Yamada, T. Balashov, A. F. Takács, R. J. H. Wesselink, M. Däne, M. Fechner, S. Ostanin, A. Ernst, I. Mertig, and W. Wulfhekel: Nat. Nanotechnol. **5** (2010) 792.
12) L. Gerhard, T. K. Yamada, T. Balashov, A. F. Takács, R. J. H. Wesselink, M. Däne, M. Fechner, S. Ostanin, A. Ernst, I. Mertig, and W. Wulfhekel: IEEE Trans. Magn. **47** (2011) 1619.
13) R. Ramesh: Nat. Nanotechnol. **5** (2010) 761.
14) T. K. Yamada, A. L. Vázquez de Parga, M. M. J. Bischoff, T. Mizoguchi, and H. van Kempen: Microsc. Res. Tech. **66** (2005) 93.
15) T. K. Yamada, M. M. J. Bischoff, G. M. M. Heijnen, T. Mizoguchi, and H. van Kempen: Jpn. J. Appl. Phys. **42** (2003) 4688.
16) W. Wulfhekel, U. Schlickum, and J. Kirschner: Microsc. Res. Tech. **66** (2005) 105.
17) R. Wiesendanger: Rev. Mod. Phys. **81** (2009) 1495.
18) V. A. Ukraintsev: Phys. Rev. B **53** (1996) 11176.
19) T. K. Yamada, M. M. J. Bischoff, T. Mizoguchi, and H. van Kempen: Surf. Sci. **516** (2002) 179.
20) T. K. Yamada, M. M. J. Bischoff, G. M. M. Heijnen, T. Mizoguchi, and H. van Kempen: Phys. Rev. Lett. **90** (2003) 056803.
21) T. Michely, M. Hohage, M. Bott, and G. Comsa: Phys. Rev. Lett. **70** (1993) 3943.
22) M. M. J. Bischoff, T. K. Yamada, C. M. Fang, R. A. de Groot, and H. van Kempen: Phys. Rev. B **68** (2003) 045422.
23) J. C. Slonczewski: Phys. Rev. B **39** (1989) 6995.
24) F. J. Jedema, A. T. Filip, and B. J. van Wees: Nature **410** (2001) 345.
25) T. Balashov, T. Schuh, A. F. Takács, A. Ernst, S. Ostanin, J. Henk, I. Mertig, P. Bruno, T. Miyamachi, S. Suga, and W. Wulfhekel: Phys. Rev. Lett. **102** (2009) 257203.